scientific reports

Check for updates

OPEN

Loss of Sirtuin 7 impairs cell motility and proliferation and enhances S-phase cell arrest after 5-fluorouracil treatment in head and neck cancer

Marta Halasa[1,2,5,6,7]✉, Syeda Afshan[2,7], Anna Wawruszak[1]✉, Agata Borkowska[3], Klaudia Brodaczewska[3], Alicja Przybyszewska-Podstawka[1,4], Joanna Kalafut[1], Marzena Baran[1], Adolfo Rivero-Müller[1], Andrzej Stepulak[1,7] & Matthias Nees[1,2,7]

Sirtuin 7 (SIRT7), a member of the sirtuin family of NAD+-dependent deacetylases, plays a vital role in cancer, exhibiting context-dependent functions across various malignancies. Our study investigates the role of SIRT7 depletion in head and neck squamous cell carcinoma (HNSCC) progression. In vitro and 3D organotypic models demonstrated that *SIRT7* knock-out attenuates cancer cell viability, proliferation, and motility as well as induces downregulation of migration- and epithelial-mesenchymal transition (EMT)-related gene expression. Moreover, the SIRT7 loss results in slower organoid formation and less invasive organoid morphology, validated by vimentin downregulation. The SIRT7 loss potentiates S-phase arrest in cell cycle progression after 5-FU treatment and elevates the ratio of dead cells. Additionally, *SIRT7* deletion reduces the expression of G1 phase-associated proteins, Cyclin D and CDK4. Altogether, our study highlights SIRT7 as a promising therapeutic target in HNSCC, enhancing the effectiveness of treatment modalities such as combinational treatment.

Keywords HNSCC, SIRT7, 5-FU, cell cycle, HDAC

Head and neck cancers constitute a heterogeneous group of tumours, where the most common are squamous cell carcinomas (HNSCCs). They are the sixth most common malignancy worldwide, affecting over 500.000 new cases annually and almost 50% – 250.000 of them – die every year[1]. The most substantial factors for the initiation and progression of HNSCC are chronic tobacco smoking and heavy alcohol consumption, especially in the case of oral cavity and larynx cancers. In contrast, pharynx cancers mainly originate from human papillomavirus (HPV) infection[2]. The overall 5-year survival rate for patients with HNSCC is relatively low due to late detection and diagnosis, as well as its invasive and metastatic nature[3]. The most common first-line strategies for primary HNSCC treatment for stage I-III cancer patients are surgical resection (for oral cavity cancers) and radiotherapy (pharyngeal and laryngeal cancers), followed by immunotherapy and chemotherapy for recurrent and metastatic HNSCC (stage IV), often administrated in combination[4]. Currently, chemotherapy is not used as first-line therapy, and for advanced treatment of HNSCC, the extreme regimen consisting of a combination of cisplatin, 5-fluorouracil (5-FU) and Cetuximab is widely used[5]. The recent meta-analysis, including 107 trials for non-metastatic, stage III and IV head and neck carcinoma patients, confirmed the benefits of induction and concomitant chemotherapy (cisplatin and 5-FU)[6].

The molecular and genetic landscape of HNSCC has been actively investigated over the past decade, introducing new molecular strategies potentially beneficial for patient treatment. Alterations in genes that affect

[1]Department of Biochemistry and Molecular Biology, Medical University of Lublin, Lublin 20-093, Poland. [2]FICAN West Cancer Centre, Institute of Biomedicine, University of Turku, Turku 20520, Finland. [3]Laboratory of Molecular Oncology and Innovative Therapies, Military Institute of Medicine, National Research Institute, Szaserow 128, Warsaw 04-141, Poland. [4]Department of Molecular Biology, Institute of Biochemistry, Faculty of Biology, University of Warsaw, Miecznikowa 1, Warsaw 02-096, Poland. [5]Transplant Immunology, The Houston Methodist Research Institute, 6670 Bertner Ave, Houston, TX 77030, USA. [6]Department of Surgery, The Houston Methodist Hospital, 6670 Bertner Ave, Houston, TX 77030, USA. [7]Marta Halasa, Syeda Afshan, Andrzej Stepulak and Matthias Nees contributed equally to this work. ✉email: mhalasa@houstonmethodist.org; anna.wawruszak@umlub.pl

cell motility, apoptosis, and cell cycle have often been found to occur in patients suffering from HNSCC[7–10]. Along with the accumulation of genetic alterations, epigenetic and posttranslational modifications have gained particular interest since they also influence tumour development and metastasis[11,12]. Epigenetic modifiers like the histone deacetylases (HDACs) remove the acetyl groups from both histones (thus tightening the chromatin structure in silenced regions) and non-histone proteins, impacting essential cell functions and eventually determining its fate[13,14]. The HDAC family consists of 18 enzymes and is divided into four groups. The third group of HDACs, called Sirtuins, has seven members (SIRT1-SIRT7). While some Sirtuin family members like SIRT1 and SIRT2 have been comprehensively studied, and selective inhibitors are available, others like SIRT7 are yet to be better understood, and there are no small molecule inhibitors commercially available specifically targeting these proteins[15]. There is limited knowledge concerning the role of SIRT7 in cancer progression, and the existing data are not comprehensive. On the one hand, some studies emphasize the oncogenic potential of SIRT7, resulting in aggressive cancer phenotypes with enhanced metastasis and poor patient prognosis[16,17]. SIRT7-mediated deacetylation of histone 3 (H3) at the lysine 18 residue (H3K18Ac) is critical for maintaining a cancer phenotype and stabilizes tumorigenicity[18]. On the other hand, SIRT7 functions as a tumour suppressor in some cancer types[19,20]. In advanced HNSCC, *SIRT7* expression has been significantly upregulated in leukocytes in preoperative and postoperative peripheral blood samples[21]. Whereas a reduction of *SIRT7* expression has been observed in patient tissues with advanced stages compared to early stages, indicating that downregulation of SIRT7 in tumour tissue might trigger tumour progression[22].

This study aims to further elucidate the functional role of SIRT7 in HNSCC and reports the novel finding that SIRT7 loss sensitizes the cells to chemotherapy. In the current research, we used two patient-derived cell lines from the University of Turku Squamous Cell Carcinoma (UT-SCC) panel: UT-SCC-24B and UT-SCC-42B, isolated from the cervical lymph node of patients suffering from recurrent tongue squamous cell and metastatic laryngeal squamous cell carcinoma, respectively. We examined the effects of *SIRT7* knock-out (SIRT7-KO) on cell proliferation, migration, and changes in phenotypic and morphological features in organoids. Additionally, we analyzed the changes following 5-FU treatment. The outcome showed a tremendous impairment in the formation of the organotypic cultures and classified SIRT7 as an HNSCC oncoprotein.

Results

SIRT7 mRNA expression is dysregulated in HNSCC, and it correlates with poor patient overall survival (OS)

To investigate *SIRT7* expression in tissue samples from HNSCC patients, we analyzed data from several open-access databases: cBioPortal (https://www.cbioportal.org), Genomic Data Commons Data Portal (https://portal.gdc.cancer.gov) and GEPIA (http://www.gepia.cancer-pku.cn). Initially, we compared mRNA expression levels of *SIRT7* in HNSCC samples and non-tumour samples (Fig. 1a). We observed higher *SIRT7* expression in tumour samples (red) compared to non-tumour ones (green). Further, we compared the overall survival (OS) rate among HNSCC patients with higher vs. lower *SIRT7* expression (Fig. 1b). We found slightly better survival for patients with a decrease in *SIRT7*. We also observed that changes in the distribution of *SIRT7* mRNA expression did not correlate with the tumor stage (Fig. 1c). Interestingly, we noticed that *SIRT7* differential expression is mutually exclusive to the expression of *SIRT1*, *SIRT2* and *HDAC1*. In other words, when *SIRT1*, *SIRT2* or *HDAC1* is overexpressed or altered, *SIRT7* remain unchanged and vice versa (Fig. 1d). All these observations prompted us to investigate the SIRT7 role in HNSCC progression. Since there are not any commercially available SIRT7 inhibitors, we employed CRISPR/Cas9 genome editing in both the recurrent (UT-SCC-24B) and metastatic (UT-SCC-42B) carcinoma cells to create a homozygous knockout of *SIRT7*, confirming SIRT7 deletion by Western blotting. To ensure biological significance, our experiments used two *SIRT7*-knockout (SIRT7-KO) clones for each cell line (Fig. 1e, f).

Loss of SIRT7 promotes inhibition of proliferation and impairs cell motility of HNSCC cells

To address whether SIRT7 potentiates or impairs cell growth, we examined cell viability and proliferation upon knock-out of *SIRT7*. Our data showed that the deletion of *SIRT7* significantly inhibited viability in both cell lines (UT-SCC-24B and UT-SCC-42B) compared to their controls. Remarkably, the decrease in metabolic activity indicated by cellular viability was consistently observed in both clones of SIRT7-KO compared to their respective controls (Fig. 2a). The proliferation analysis yielded similar results, with both cell lines exhibiting a slower proliferation rate than their controls (Fig. 2b). Further, we analyzed how the *SIRT7* knock-out affects cell motility by performing a wound healing (scratch) assay followed by expression analysis of genes strongly associated with cell movement and, simultaneously, confirmed to be involved in HNSCC progression[23–25]. Our findings revealed that SIRT7-KO clones exhibited decreased migration for both cell lines compared to their respective controls (Fig. 2c, d). In line with this observation, we found that *CD44*, *Fibronectin (FN1)*, and *TWIST1* mRNA levels were downregulated for SIRT7-KO clones compared to their controls in both cell lines (Fig. 2e, f,g). Intriguingly, while we observed significant SIRT7-KO-mediated downregulation of *N-cadherin* (*CDH2*) expression in UTSCC42B, the level of *CDH2* in UT-SCC-24B remained unchanged (Fig. 2h). Thus, we examined the *E-cadherin (CDH1)* mRNA levels for the UT-SCC-24B line and observed an increase in its expression in SIRT7-KO clones compared to the control (**Supplementary Fig. 1**).

Knock-out of *SIRT7* inhibits the growth of organoids and affects their morphology

To validate 2D data, we generated a 3D organotypic model. The single cells started to replicate and form organoids in 4 days from cell seeding for controls and SIRT7-KO clones of both the UT-SCC cell lines. However, over time, there was a significant inhibition of the growth of organoids in SIRT7-KO clones of both cell lines compared to their controls (Fig. 3a). After 10 days in culture, the organoids were stained with live cell dye, Calcein AM. As expected, *SIRT7* deletion caused a significant decrease in cell viability (Fig. 3b) as well as changes in morphometric

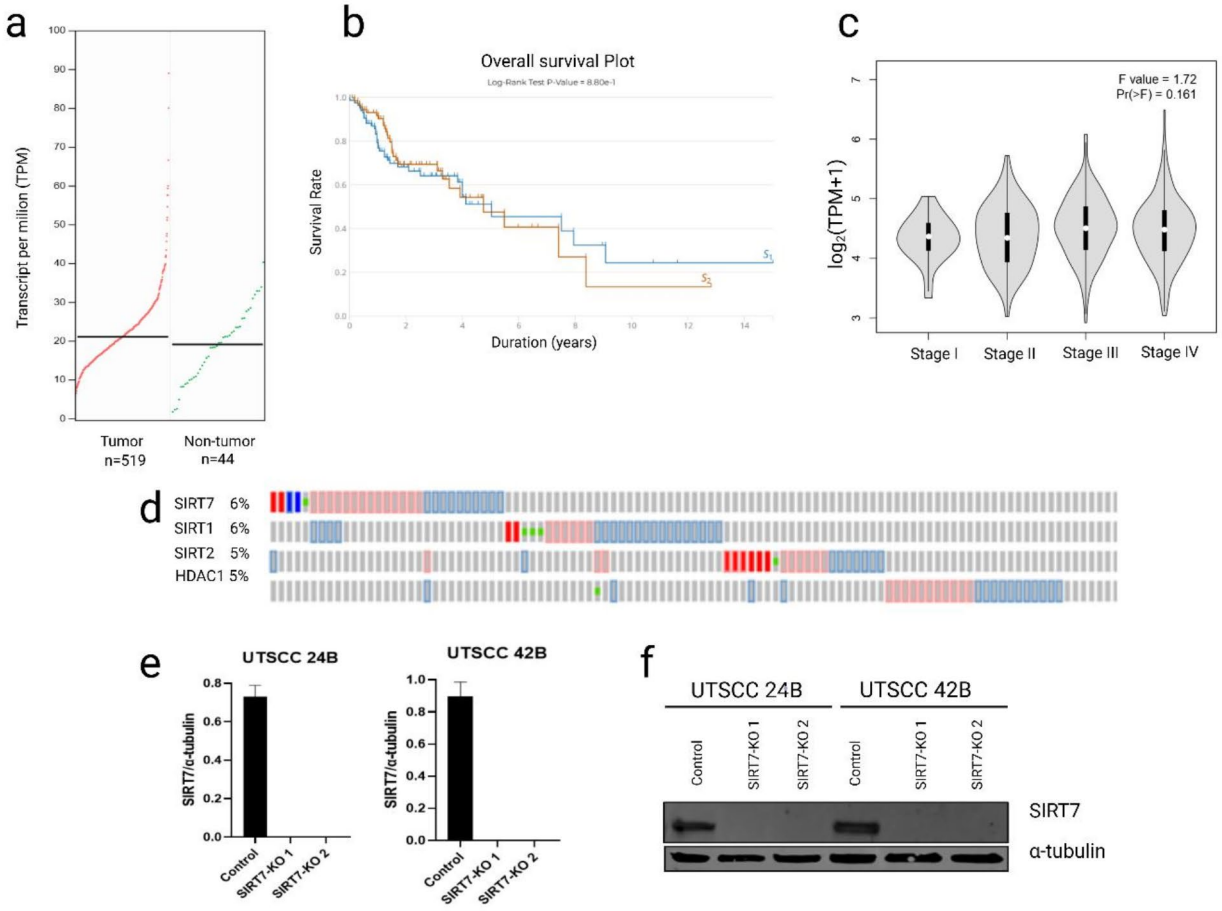

Fig. 1. SIRT7 acts as an oncogene in patients with head and neck squamous cell carcinoma (HNSCC). The relative *SIRT7* expression in HNSCC tissues (red) and non-tumour tissues (green) (**a**). The Kaplan-Meier survival plot for HNSCC patient groups with high SIRT7 (red) vs. lower SIRT7 (blue) expression (**b**). The expression level of the *SIRT7* gene in different stages of HNSCC; TPM – transcripts per million (**c**). The part of plot showing genetic alterations for *HDAC1*, *SIRT1*, *SIRT2* and *SIRT7* among HNSCC patient samples; green dot – missense mutation red – amplification, blue – deep deletion, red frame – mRNA high, blue frame – mRNA low, grey – no alteration (**d**). The confirmation of *SIRT7* knockout in two cell lines, UT-SCC-24B and UT-SCC-42B, is shown as the ratio between SIRT7 and α-tubulin (loading control) (**e**). Representative blots of SIRT7 expression level across two independent repetitions.

properties such as size, shape, and texture of the organoids (Fig. 3c). The organoids grew faster and significantly larger as computed by their Area (in pixels) in control compared to the SIRT7-KO clones in both cell lines (Fig. 3d). For UT-SCC-24B, we observed that SIRT7-KO organoids presented a significantly higher percentage of differentiated round organoids than their control, while for UT-SCC-42B, the effect was the opposite (Fig. 3e). Both cell lines showed a reduced length of cell motility-related appendages/protrusions (MedApp in pixels) in organoids, yet the effect was more profound for the UT-SCC-24B cell line (Fig. 3f). The higher percentage of roundness and decreased number of appendages/protrusions are indicative of less pronounced invasion dynamics and reduced cell motility[26]. The control organoids with parental SIRT7 expression had a more irregular shape with a larger number of multicellular protrusions (**arrows in** Fig. 3c), indicating increased growth and invasiveness. Further, we investigated the expression of vimentin, an established marker of mesenchymal trans-differentiation in epithelial cancer cells (EMT), and often associated with increased invasiveness in HNSCC[27]. The SIRT7-KO led to a marked decline in vimentin expression compared to the respective controls in both cell lines (Fig. 3g, h). This observation, at least partly, might explain the observed decrease in the invasive phenotype of the SIRT7-KO organoids. Collectively, these results show that the depletion of SIRT7 diminishes cancer cell growth and tumour cell motility and invasion in both 2D and 3D conditions, suggesting that SIRT7 acts as an oncoprotein in advanced HNSCC.

Knock-out of *SIRT7* blocks S-phase progression in cell cycle progression after 5-FU treatment

In the light of the significant decrease in cellular viability and proliferation observed upon SIRT7 depletion in both 2D and 3D models, we investigated its potential influence on cell cycle progression in these cell lines. Concurrently, considering the continued use of 5-FU as a standard treatment for HNSSC patients, we evaluated

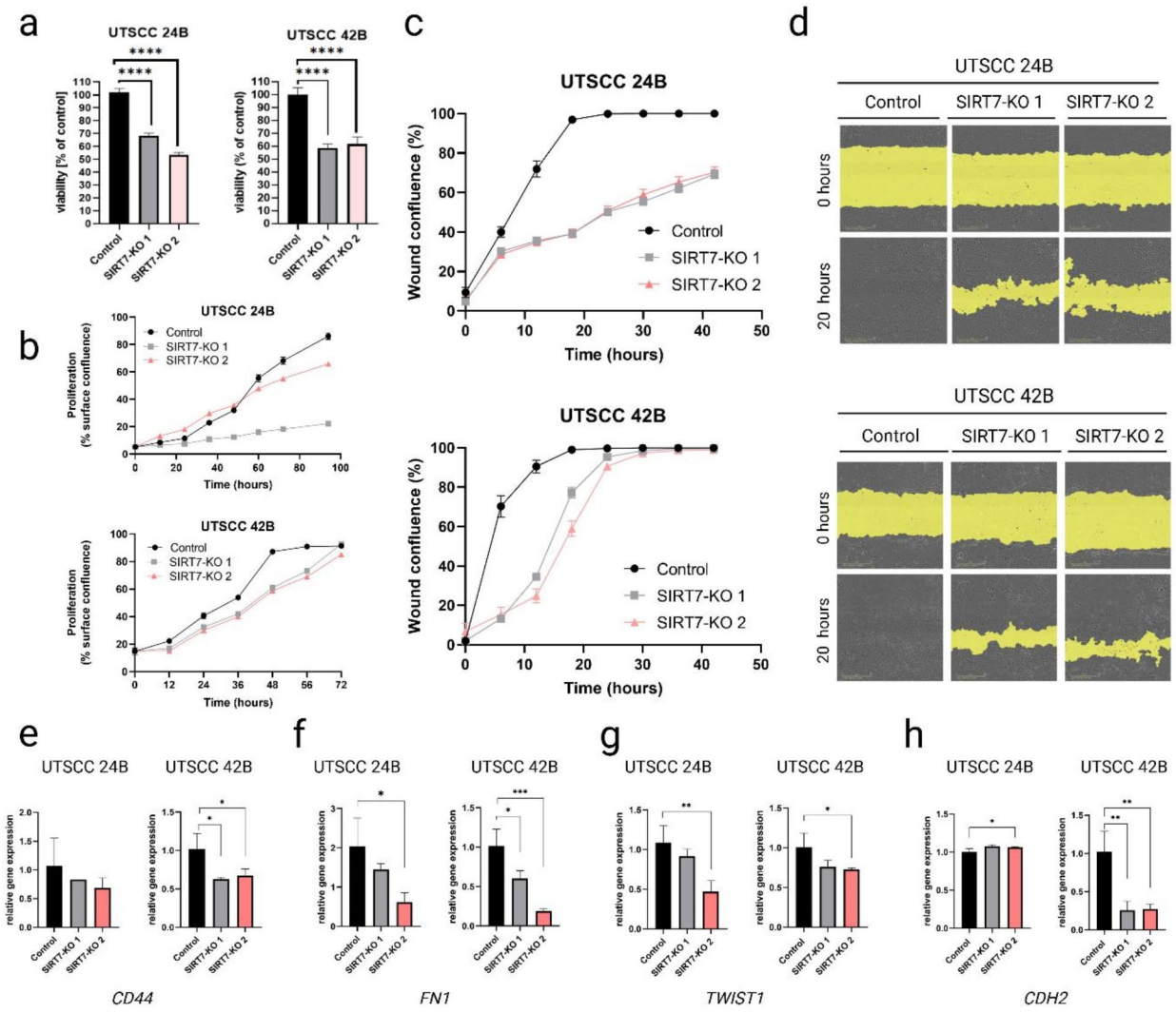

Fig. 2. Deletion of *SIRT7* impairs UTSCC cell proliferation and motility. Cell viability is assessed by the CTG assay. The graphs illustrate changes in viability between SIRT7-KO clones (UT-SCC-24B and UT-SCC-42B) and their controls, expressed as a percentage of the control. A *t*-test was used for statistical analysis (* $p < 0.05$, ** $p < 0.01$, *** $p < 0.001$, **** $p < 0.0001$) (**a**). The diagrams present changes in cell proliferation as the percentage of surface confluence in a time-dependent manner between *SIRT7*-KO clones (UT-SCC-24B and UT-SCC-42B) and their controls (**b**). The plots represent time-dependent changes in wound confluence between *SIRT7*-KO clones (UT-SCC-24B and UT-SCC-42B) and their controls (**c**). Representative pictures of wound closure at two-time points: 0 h (pictures taken immediately after a made scratch and after 20 h (pictures taken when controls reach full confluence) across three independent repetitions (**d**). The bar plots show the relative gene expression across a set of four genes: *CD44* (**e**), *Fibronectin* (*FN1*) (**f**), *TWIST1* (**g**), and *N-cadherin (CDH2)* (**h**) normalized to *GAPDH*. For statistics, the ordinary one-way ANOVA with multiple comparisons was used (* $p < 0.05$, ** $p < 0.01$, *** $p < 0.001$, **** $p < 0.0001$).

the effects of *SIRT7* KO on cell lines treated with 5-FU. We determined IC_{50} values for each cell line separately. We found that IC_{50} values for SIRT7-KO clones in both cell lines (2.98 µg/ml and 3.49 µg/ml for UT-SCC-24B SIRT7-KO1 and SIRT7-KO 2 respectively, and 1.67 µg/ml and 2.03 µg/ml for UT-SCC-24B SIRT7-KO1 and SIRT7-KO 2, respectively) are lower than controls (10.53 µg/ml and 9.47 µg/ml for UT-SCC-24B and UT-SCC-42B, respectively) suggesting SIRT7 KO might make these cells more susceptible to 5-FU treatment (**Supplementary Fig. 2**). The analysis of cell cycle progression revealed that in UT-SCC-24B, deletion of *SIRT7* led to a reduction of cells entering the S phase while showing a slight upregulation of cells in the G1 phase compared to the control. Interestingly, the proportion of cell cycle phase distribution was reversed after 5-FU treatment. 5-FU treatment caused the general upregulation of cell number in the M2 phase and downregulation of the M1 phase across all cells, the SIRT7-KO clones showed significant S phase arrest while the S phase in control remained unchanged (Fig. 4a, b). In UT-SCC-42B, both SIRT7-KO clones and the control group demonstrated a consistent pattern in the distribution of cell cycle phases. However, after 5-FU treatment, we

observed a significant cell accumulation in the S-phase of SIRT7-KO clones compared to the control (Fig. 4c, d). We further investigated the expression of cyclins and cyclin-dependent kinases (CDKs), which are prognostic markers in cancer progression[28,29]. We observed a significant downregulation of Cyclin D expression after 5-FU treatment in the SIRT7-KO clones in both cell lines, reaching statistical significance for UT-SCC-42B compared to untreated cells (Fig. 4e). We also noticed a general tendency to downregulate expression of CDK4 in 5-FU-treated cells compared to their untreated controls, regardless of SIRT7 depletion for both cell lines (Fig. 4g). A similar tendency was observed for Cyclin B expression in both cell lines, yet it is to be noticed that in UT-SCC-42B, the inhibition of Cyclin B was more profound for control (control (-) vs. control (+)) compared with SIRT7-KO clones (SIRT7-KO (-) vs. SIRT7 (+)) (Fig. 4h). UT-SCC-24B cells displayed a minor CDK1/2 expression elevation in SIRT7-KO clones post-5-FU treatment compared with control (control (-) vs. control (+)), while in UT-SCC-42B, a downward trend was observed across both control and SIRT7-KO clones, with no marked distinction between them (Fig. 4i). Overall, the findings suggest that loss of *SIRT7* affects cell cycle progression and the response to chemotherapy, with a lower concentration of 5-FU in SIRT7-KO clones, generally having a similar effect to control cells treated with a higher 5-FU concentration. Additionally, S-phase arrest is observed in SIRT7-KO clones after drug administration, indicating an impact of SIRT7 depletion on cell cycle regulation in response to chemotherapy.

5-FU treatments further decrease cell growth of SIRT7-KO and increase cell death in 3D cultures

To assess whether the absence of SIRT7 enhances the chemotherapeutic treatment effects, we administered 5-FU to 3D organotypic cultures at concentrations determined to be effective (IC_{50} values) in prior experiments. The cells seeded into Matrigel formed organoids within 4 days, after which 5-FU treatment was started. We refreshed the media, supplemented with 5-FU, every two days until the end-point on day 10. At the end-point, the organoids were stained with live cell dye Calcein AM (green stain) and dead cell marker Ethidium homodimer-2 (red stain) (**Supplementary Fig. 3**). As anticipated, we observed a notable reduction in the area (measured in pixels) of organoids treated with 5-FU compared to solvent control, depicted in the representative brightfield microscopy images (Fig. 5a). The decrease in the growth and size of organoids was regardless of *SIRT7* deletion in the UT-SCC-24B and UT-SCC-42B. Moreover, the size of organoids (area) from SIRT7-KO cells treated with 5-FU was significantly smaller than that of their respective untreated controls (Fig. 5b). We also quantified the relative amount of red fluorescence (cell death) in these multi-organoid cultures indicated by the image-related parameter AreaRatioR (in %). This parameter indicates there is a significantly higher percentage of dead cells in the organoids upon 5-FU treatment compared to the respective controls ($p < 0.0001$), irrespective of SIRT7 expression. Along with the phenotypic measures, the treatment also affected the metabolic activity of the cells, which is seen by the marked reduction in treated samples compared to untreated ones. There was only a slightly reduction of viability observed in control cells compared to SIRT7-KO clones (Fig. 5c). This suggests that lower dosages of 5-FU (as used for SIRT7-KO clones) may generate similar effects compared to higher dosages when SIRT7 is absent. A similar pattern for organoid degradation following 5-FU treatment was observed in the UT-SCC-42B cell line. The area (size) of the organoids indicating their growth was significantly decreased regardless of *SIRT7* deletion, yet 5-FU treated SIRT7-KO clones showed more profound morphometric changes and less active cells.

To investigate if the effect of 5-FU treatment on SIRT7-KO clones could be compensated by other sirtuins sharing nuclear localisation with SIRT7, we analysed their gene expression level after treatment. We observed that the mRNA expression for *SIRT1*, *SIRT2*, and *SIRT6* largely remained unchanged after *SIRT7* deletion in UT-SCC-24B. However, 5-FU treatment incluced significant downregulation of *SIRT1* in SIRT7-KO clones, while the levels of *SIRT1* remained unchanged in control. *SIRT2* is downregulated in both the clones and the control after 5-FU treatment. The *SIRT6* expression shows significant downregulation after treatment in control samples, whereas it is upregulated in a SIRT7-KO clones (**Supplementary Fig. 4a**, **b**,**c**). In UT-SCC-42B, the mRNA expression for *SIRT1*, *SIRT2*, and *SIRT6* is mostly unaffected upon *SIRT7* deletion. However, these genes are significantly downregulated after 5-FU treatment in the control and SIRT7-KO (**Supplementary Fig. 4d**, **e**,**f**).

Discussion

Decades of research have confirmed the prominent role of reversible acetylation in tumorigenesis and metastasis, and outlining the fundamental role of HDACs that mediate this process. These findings have gained the interest of researchers, pharmaceutical companies, and medical practitioners. Among all HDACs, SIRT7 remains the most underinvestigated member. Its upregulation is associated with an aggressive phenotype and correlates with poor disease outcomes in prostate, breast, and hepatocellular carcinoma (HCC)[30–34]. Mechanistically, SIRT7 deacetylation of H318Ac has been found to favour oncogenic transformation[18] Conversely, other studies propose the anti-tumour role of SIRT7 by impeding epithelial-mesenchymal transition (EMT) in breast cancer in various in vivo models and suppressing proliferation and cell motility while enhancing apoptosis in bladder cancer[35,36].

In HNSCC, the role of SIRT7 is complex and probably ambiguous. On the one hand, the downregulation of SIRT7 has been shown to facilitate tumour progression[22]. On the other hand, SIRT7 expression was associated with increased stromal lymphocyte infiltration, suggesting its involvement in influencing the invasiveness of the cancer[30]. Despite conflicting findings, the frequent occurrence of *SIRT7* genomic alterations and its substantial overexpression, on par with the most abundant family members such as *SIRT1* and *HDAC1*, intrigued us to investigate its role in HNSCC.

To address whether SIRT7 plays an oncoprotein in HNSCC progression, SIRT7-KO in vitro model using patient-derived cell lines were used to test the effects of SIRT7 on functional and phenotypical characteristics of the cells. We observed a 40% reduction in cell viability and a significant decrease in cell proliferation in SIRT7-KO clones that was similar to the reduction previously confirmed in prostate and hepatocellular carcinoma

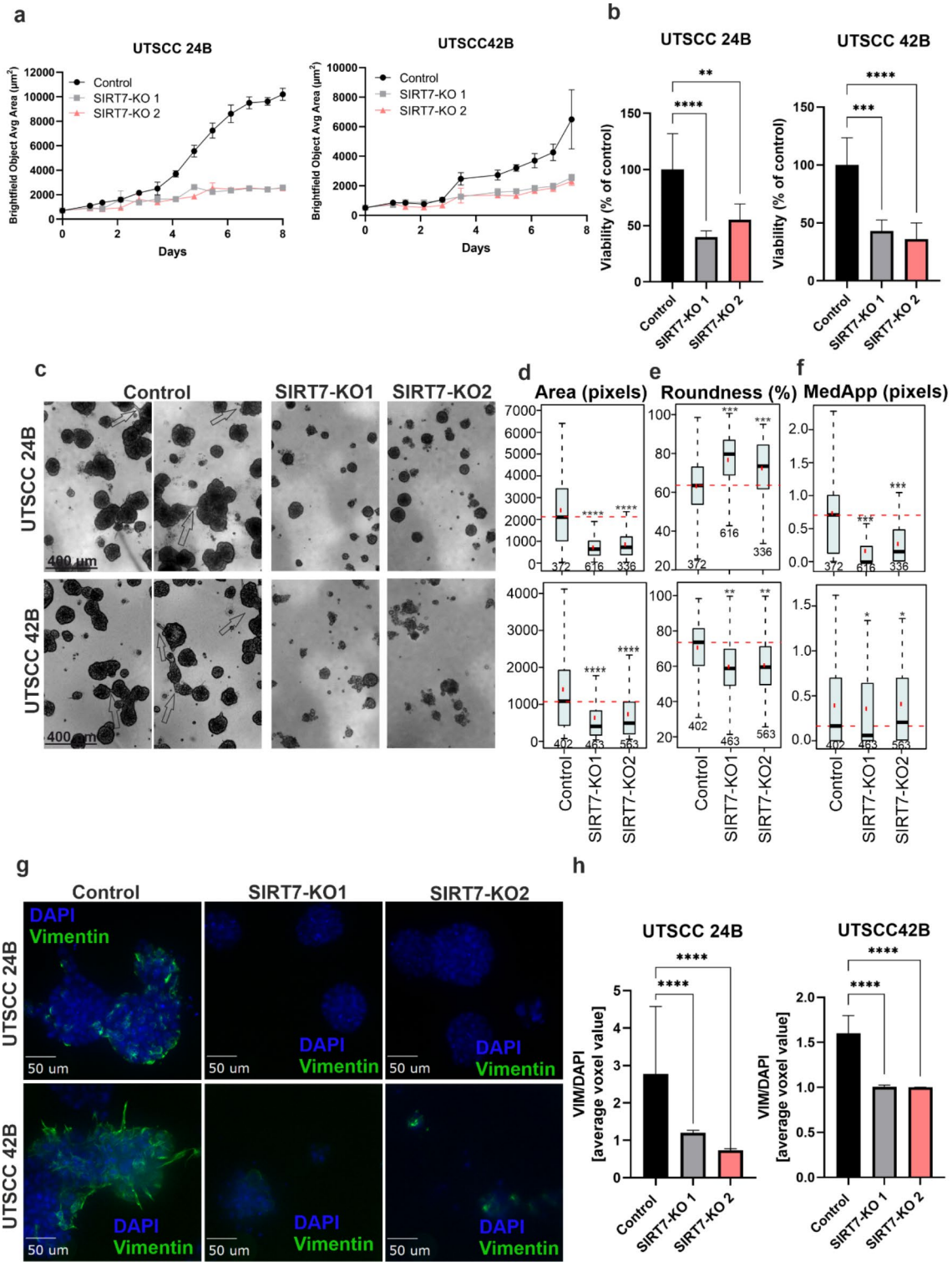

(HCC)[37,38]. The loss of *SIRT7* also inhibited tumor cell motility and invasiveness, which is often associated with an active EMT. Thus, we specifically investigated altered expression of genes involved in cell motility, which may be simultaneously engaged in HNSCC progression, and potentially critical for EMT. We observed the significant downregulation of *CD44*, *Fibronectin*, and *Twist1* gene expression in SIRT7-KO lines. This is in line with the observation that in patient samples, *CD44* and *Fibronectin* were significantly upregulated in HNSCC tissues and correlated with poor survival[39,40]. Moreover, *Twist1* was found to promote EMT through downregulation of E-cadherin (*CDH1*) in esophageal squamous cell carcinoma (ESCC)[41]. E-cadherin to N-cadherin (*CDH2*) switching is a significant marker in the EMT in HNSCC, which we observed in UT-SCC-42B SIRT7-KO clones[42]. Meanwhile, in UT-SCC-24B SIRT7-KO clones, the *CDH2* mRNA level remained unchanged, and *CDH1* was upregulated. Overall, these data showed that *SIRT7* deletion suppresses cancer cell growth and migration, suggesting that SIRT7 could act as an oncoprotein. Yet, another published report observed that high expression

◀**Fig. 3**. *SIRT7* KO represses HNSCC growth in 3D organotypic cultures. After organoid formation (4 days), the area of organoid growth is reduced in SIRT7-KO clones compared to the control in UT-SCC-24B and UT-SCC-42B cells (**a**). Significant decrease in proliferation and viability upon loss of *SIRT7* in UT-SCC-24B and UT-SCC-42B KO clones and controls. One-way ANOVA using Dunnett's test of $n = 3$ replicas (* $p < 0.05$, ** $p < 0.01$, *** $p < 0.001$, **** $p < 0.0001$) (**b**). Representative brightfield microscopy images of the 3D organoids on day 10 of culture. The arrows indicate the protrusions or appendages from the organoids. Scale bar of 400 µm (**c**). The box and whisker plots show the median size, shape, and appendages of the organoids (black horizontal line), the median size, shape and appendages of the control (dotted red horizontal line), and the total number of objects in the analyses under the box plot. Statistical significance of $n = 3$ replicas calculated using Bonferroni-corrected *t*-test (* $p < 0.05$, ** $p < 0.01$, *** $p < 0.001$, **** $p < 0.0001$) (**d**, **e**,**f**). Immunofluorescence staining of the 3D organoids using Vimentin (green) and nuclei counterstained with DAPI (blue). The merged Z-stack images from confocal microscopy are displayed with a scale bar of 50 µm (**g**). The graphs represent a significant decrease in Vimentin (VIM) and DAPI ratio upon *SIRT7* deletion from both cell lines. For statistical analysis, the ordinary one-way ANOVA with multiple comparisons was used (* $p < 0.05$, ** $p < 0.01$, *** $p < 0.001$, **** $p < 0.0001$) (**h**).

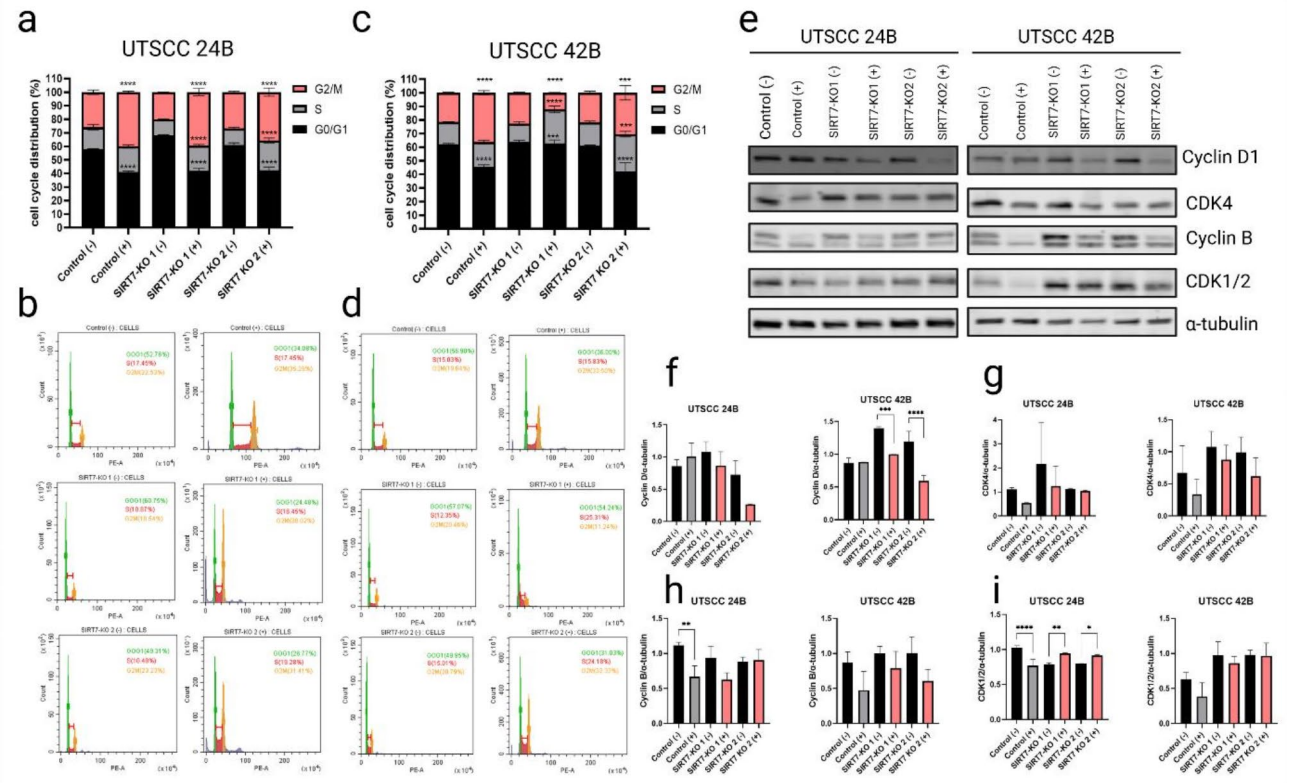

Fig. 4. SIRT7-KO induces S-phase arrest after 5-FU treatment.*SIRT7* loss itself does not affect the cell cycle progression, as indicated by the use of flow cytometry after 48 h of drug treatment. The use of lower dosages of 5-FU (IC_{50} values determined for each cell line) showed similar cell cycle arrest in the G2/M phase in SIRT7-KO for UT-SCC-24B clones and SIRT7-KO2 for UT-SCC-42B compared to control. For all clones (both cell lines), the use of lower values of 5-FU induces cell cycle arrest in the S phase compared to the control, where 5-FU concentration was higher. (-) indicates untreated cells (DMSO) and (+) are treated cells with IC_{50} value of 5-FU. For statistics, two-way ANOVA with multiple comparisons was used (* $p < 0.05$, ** $p < 0.01$, *** $p < 0.001$, **** $p < 0.0001$). To keep the graphs readable, we implemented statistics for treated and untreated samples within one cell line. The statistics between different cells (clones vs. control) are attached as **Supplementary Table 3**. The representative flow cytometry charts across three independent repetitions for UT-SCC-24B and UT-SCC-42B (**b**, **d**). The representative blots across three independent repetitions for UT-SCC-24B and UT-SCC-42B after 48 h 5-FU treatment for Cyclin D1, CDK4, CyclinB, CDK1/2, and α-tubulin used as a loading control (**e**). The graphs show changes in proteins expression (normalized to α-tubulin) after 48 h of 5-FU treatment inUT-SCC-24B and UT-SCC-42B cells. For statistics, the one-way ANOVA with multiple comparisons was used (treated vs. untreated cells) (* $p < 0.05$, ** $p < 0.01$, *** $p < 0.001$, **** $p < 0.0001$) (**f**, **g**,**h**, **i**).

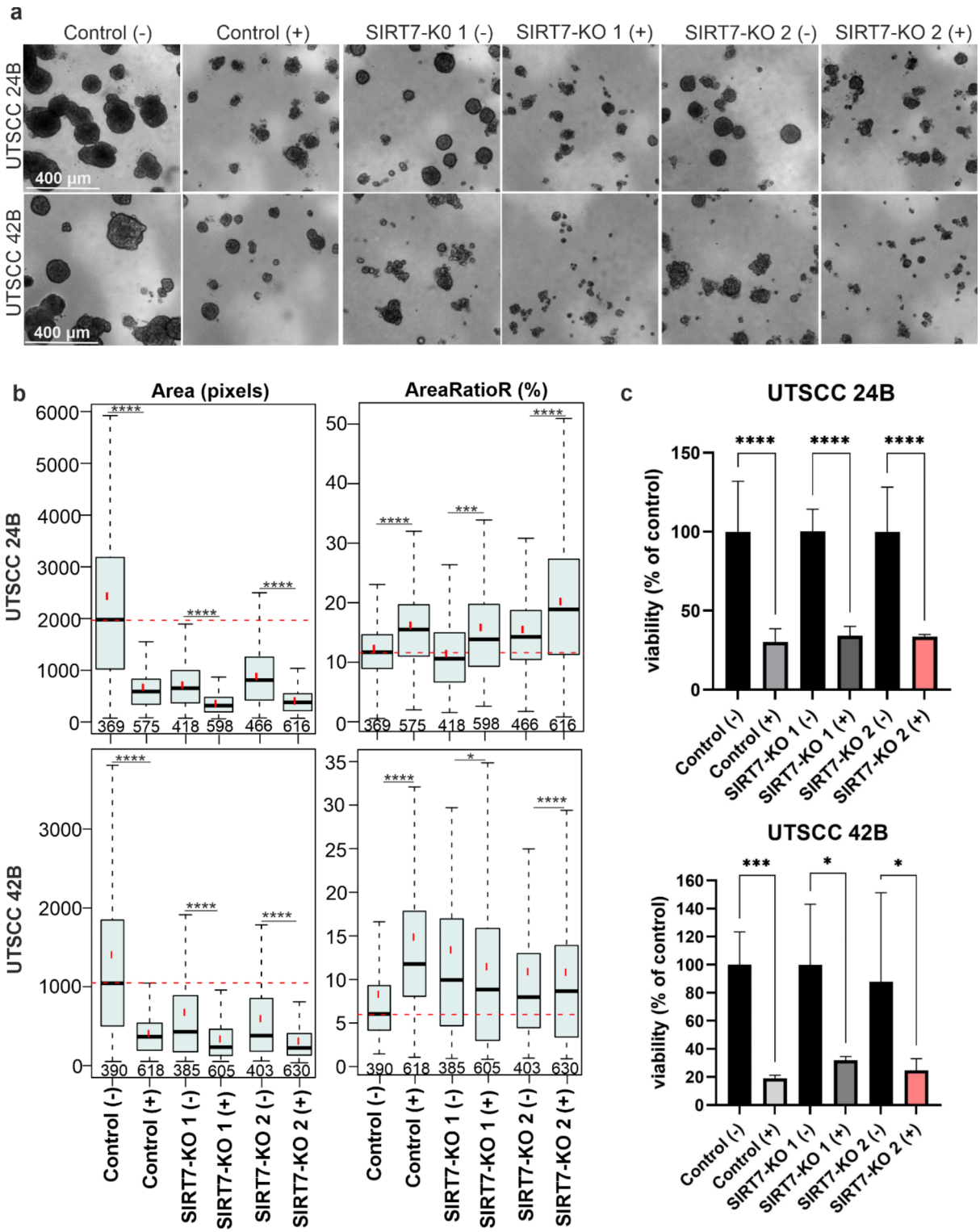

Fig. 5. *SIRT7* deletion enhanced a decrease in organoid prosperity after 5-FU treatment. Brightfield images with 10x objective and scale bar of 400 µm. These indicate the condition of the organoids with IC50 5-FU treatment (+) and with solvent control (-) in control and SIRT7-KO clones (**a**). The quantitative measure of the 5-FU treatment with (+) and without (-) IC50 of the drug. The box and whisker plots show the median size (area) and the ratio of dead cells (AreaRatioR) in the organoids (black horizontal line), the median size of untreated control (dotted red horizontal line), and the total number of objects in the analyses under the box plot. Statistical significance of $n = 3$ replicas calculated using Bonferroni-corrected *t*-test (* $p < 0.05$, ** $p < 0.01$, *** $p < 0.001$, **** $p < 0.0001$) (**b**). The effect on cellular viability of the organoids after 6 days of treatment with 5-FU. One-way ANOVA using Dunnett's test of $n = 3$ replicas (* $p < 0.05$, ** $p < 0.01$, *** $p < 0.001$, **** $p < 0.0001$) (**c**).

levels of SIRT7 may reduce HNSCC metastasis by suppressing EMT[43]. Since the role of SIRT7 in cancer is complex, cellular- and context-dependent, the different origins of the cell lines in this study could, at least partly, explain these opposite effects. SIRT7 expression and activity may strongly depend on the context, the genetic mutation background of the tumor cells, and their differentiation status.

In the more physiologically representative 3D model, we observed a slower rate of organoid formation along with morphological changes such as a reduction in the size of the SIRT7-KO organoids coupled with lower metabolic viability compared to controls. The irregular morphology of control organoids that show more protrusions and a less round may signify poorly differentiated organoids with a heightened invasion potential, compared to the more round, more differentiated, and less invasive SIRT7-KO organoids[26]. This could correlate with a significant decrease in vimentin expression observed in SIRT7-KO clones, which is in line with another report demonstrating that overexpression of SIRT7 was associated with upregulation of vimentin expression and increased invasion in colorectal cancer[32,44].

We further tested whether SIRT7-KO-mediated reduction in proliferation could be associated with changes in the cell cycle progression. It has been reported that SIRT7 is required for p53-dependent cell cycle arrest in the G1 phase[45]. *TP53* is one of the most frequently mutated genes in HNSCC. Therefore, we would speculate that this functional link may provide an alternative explanation through which SIRT7 modulates the cell cycle progression in HNSCC[46]. Our data indicate that *SIRT7* deletion caused a general reduction in the S phase progression during cell cycle progression. A similar result was observed when *SIRT7* was knocked down in non-small cell lung cancer, indicating that SIRT7 may facilitate tumour progression through cell cycle regulation[47]. The involvement of SIRT7 in cell growth and its importance in promoting or facilitating entry into the S phase could be associated with its ability to regulate DNA replication and repair. SIRT7 has been linked to DNA damage response by indirectly promoting non-homologous end joining (NHEJ) DNA repair, and thus promoting genome stability[48]. To investigate whether other sirtuins can compensate for the SIRT7-KO, we analysed mRNA levels of *SIRT1*, *SIRT2* and *SIRT6* before and after treatment. In patients with acute myeloid leukaemia, a significant positive correlation between certain sirtuins, particularly between *SIRT2* and *SIRT7*, and *SIRT6* and *SIRT7* was reported[49]. Our data showed that sirtuin levels were largely unaffected by SIRT7-KO in both cell lines. However, in UT-SCC-24B, the expression of S*IRT1* was significantly downregulated after 5-FU administration in SIRT7-KO clones compared to the control. Interestingly, *SIRT1* overexpression is associated with a good prognosis in HNSCC patients[50]. In UT-SCC-42B, *SIRT1*, *SIRT2*, and *SIRT6* were significantly downregulated after treatment in controls and SIRT7-KO clones, suggesting that expression patterns of these sirtuins can be stage- and phenotype-dependent.

We also addressed whether SIRT7-KO could affect cell cycle distribution following 5-FU treatment. As a pyrimidine analogue, 5-FU is well known to induce S-phase arrest in HNSCC[51]. We observed a significant enhancement in 5-FU-mediated S-phase arrest in SIRT7-KO clones, whereas a similar effect was not found in the controls. The lower IC_{50} observed for 5-FU in SIRT7-KO cells compared to control cells suggests that lack of SIRT7 makes these HNSCC cell lines more susceptible to the growth-inhibitory effects of 5-FU. Moreover, we observed a similar pattern for G1 phase reduction after 5-FU treatment for both controls and SIRT7-KO clones, which partly confirms the SIRT7-KO mediated sensitization. The reduction of the number of cells in the G1 phase is indicative of decreased tumorigenesis, especially since 5-FU is accompanied by the general downregulation of G1 master regulators Cyclin D and CDK4 in SIRT7-KO clones upon treatment[52]. Notably, the area (=size) of the organoids in SIRT7-KO clones was significantly further reduced after 5-FU treatment compared to both untreated SIRT7-KO clones and controls. Simultaneously, there was an increase in the ratio of dead cells (stained ethidium homodimer) in 5-FU treated SIRT7-KO clones compared to 5-FU treated control in UT-SCC-24B. In UT-SCC-42B, while the use of 5-FU did not increase the dead cell in 5-FU treated SIRT7-KO clones, we found that SIRT7-KO itself elevates the ethidium homodimer positive cells. The data from 3D organoid cultures partly confirm the potential SIRT7-KO mediated sensitization to 5-FU treatment. Lower 5-FU dosages induced a similar or more pronounced effect in SIRT7-KO clones than the high dosage of 5-FU used in the control treatment. This is indicated by the general reduction of growth and decreased morphological irregularity observed already at the beginning of organoid formation.

However, the exact mechanism for these phenotypic changes should be more deeply investigated, including genome-wide expression analyses.

Conclusions

SIRT7 plays an important, cancer-type dependent role in cancer progression and metastasis. Our research indicates a potential tumorogenic role in HNSCC, suggesting that SIRT7 could be a potential target in anti-cancer therapy. The observed susceptibility to 5-FU treatment in SIRT7-deleted cells suggests that targeting SIRT7 could enhance the efficacy of existing chemotherapy regimens. Downregulation or inhibition of SIRT7 activity could benefit patients suffering from HNSCC, yet the FDA has not approved any sirtuin inhibitors to date, and the first selective SIRT7 inhibitor has been reported only recently but is not commercially available for academic research[53,54]. While our study contributes to a better understanding of the role of SIRT7 in cancer progression, it also emphasizes the need for further research to unravel the full spectrum of its complex functions and the regulatory mechanisms it may be involved in. Future studies should explore the possibility of targeting SIRT7 in combination with other therapeutic agents, including immunotherapeutics, to maximize treatment efficacy and minimize potential adverse effects.

Methods

Cell culture

UT-SCC-24B (RRID: CVCL_7826) and UT-SCC-42B (RRID: CVCL_7848) were kindly received from Prof. Reidar Grénman group at the University of Turku, Finland. Cells were authenticated using short tandem repeat profiling at IdentiCell Laboratories (Department of Molecular Medicine at Aarhus University Hospital Skejby, Århus, Denmark). They were routinely tested for mycoplasma (Lonza LT07-118 mycoplasma detection kit) while in culture. Cells were transfected to generate stable knockout clones according to the method described in Sect. 5.2. UT-SCC-24B and UT-SCC-42B cells were cultured at 37 ˚C, 5% CO_2 in growth media DMEM with high glucose and GlutaMAX™ Supplement (ThermoFisher Scientific, US) supplemented with 10% fetal bovine serum (FBS; ThermoFisher Scientific, USA), 0.4 µl/ml hydrocortisone (Merck, Germany), and 100 Units/ml of Potassium Penicillin and 100 µg/ml of Streptomycin Sulfate (Lonza Bioscience, USA). The drug, 5-fluorouracil (5-FU) was purchased from Selleck Chemicals (NSC 19893, US).

Transfection and generation stable knock-out

The CRISPR-Cas9 genome editing technique was employed to generate stable *SIRT7* knock-out HNSCC cell lines. Two guide RNA (gRNA) sequences were design using the CRISPOR and Benchling (https://www.benchling.com) online platform and subsequently ordered as a synthetic DNA fragments flanked BbsI recognition site[55]. These sequences: TTTGGCGTTCCGGACGGCGC and CGCAGGTGTCGCGCATCCTG were ligated into pSpCas9(BB)-2A-Puro (PX459) V2.0 vector, generously provided by Feng Zhang (Addgene plasmid # 62988 ; http://n2t.net/addgene:62988 ; RRID: Addgene_62988). The cloning process utilized the Golden Gate Assembly[56]. Cell lines (UT-SCC-24B and UT-SCC-42B) were seeded at density 5×10^4 cells/well into a 24-well plate 24 h before transfection. Using Lipofectamine 3000® transfection reagent following the manufacturer's protocol, cells were transfected with pSpCas9(BB)-2A-Puro (PX459) V2.0 with guide RNA (gRNA) vector. Transfection with plasmid pSpCas9(BB)-mCardinal-2A-Puro without gRNA, created in our laboratory for the visualization of Cas9-expressing cells, was employed and used as a negative control. After 48 h, cells were selected with Puromycin (1 µg/ml) for over three weeks to generate stable lines. Following selection, individual cell colonies were seeded into separate wells. PCR amplification was conducted to screen for modified cells compared to the control, using the following primers: forward 5'-ACCTTTTAAAGAGACTGGCAGG-3' and reverse 5'-GAGTTTTTCGCGATTACTGGAG-3'. All mutant clones were validated by sequencing of the genomic DNA using primer 5'-ACCTTTTAAAGAGACTGGCAGG-3'. To confirm *SIRT7* knockout, Western blot analyses were performed.

2D cell proliferation and viability assay

The UT-SCC-24B and UT-SCC-42B SIRT7-KO clones and controls were seeded in a 96-well plate at a density of 0.5×10^4 cells/well in the growth media. Once the cells adhered overnight, the cells were imaged every 12 h using Incucyte® S3 live cell imager (Sartorius Stedim Biotech, France). The proliferation was monitored for 3 days after seeding and the data from phase-contrast images were segmented and analyzed with the Incucyte® S3 software. The Cell Titre Glo 2.0 metabolic viability assay (Promega, USA) was used according to the manufacturer's protocol to measure the difference between cellular viability across the controls and SIRT7-KO cells. The luminescence of cells was measured using the VICTORX Light Luminescence Microplate Reader (Perkin Elmer, USA).

Determination of IC50 values

Cells were seeded on a 96-well plate at a density of 1.0×10^4 cells/well. The following day, cells were exposed to serial dilutions of a total concentration of 5-FU (controls: 0.1–25 µg/ml, SIRT7-KO clones: 0.1–10 µg/ml) for 48 h. After 48 h, the Titre Glo 2.0 assay (Promega, USA) was used according to the manufacturer's protocol. The luminescence was measured using an Infinite M200 Pro microplate reader (Tecan, Männedorf, Switzerland). Dose-response curves were plotted to determine half-maximal inhibitory concentrations (IC_{50}) for the compound 5-FU, using GraphPad Prism 9.0 (GraphPad Software, San Diego, CA, USA).

Wound healing assay

Cells were seeded on a 96-well plate at a density of 1.0×10^4 cells/well. After they reached complete confluence, a wound in the form of a scratch was made uniformly in each well using the Incucyte® Woundmaker Tool (Sartorius, Germany). The cells were washed twice with phosphate-buffered saline (PBS) (ThermoFisher, USA), and fresh growth medium was added with and without drug treatment (IC_{50} of 5-FU). The cell plate was monitored using IncuCyte S3 imaging system (Sartorius, Germany) until the wound was closed. The time-dependent, wound confluence was quantitated and analyzed using the IncuCyte S3 software.

Quantitative reverse transcriptase-polymerase chain reaction (qRT-PCR)

The controls and SIRT7-KO clones for both the cell lines were seeded on a 6-well plate at a density of 5.0×10^5 cells/well in complete media. The cells were cultured until 60% confluence. In the case of 5-FU treatment, the following day after seeding, the culture medium was replaced with the medium containing 5-FU (IC_{50} as mentioned in Sect. 5.3.1) and incubated for 48 h. After 48 h, cells were harvested, and total RNA was extracted with the RNeasy Mini Kit (Qiagen, Germany). A concentration of 1 µg of RNA was used to make complementary DNA with a mix of dNTP (Thermo Fisher Scientific, Finland), Oligo dT primer (Oligomer Oy, Finland), RNase inhibitor (Promega, USA) and Maxima reverse transcriptase (Thermo Fisher Scientific, Finland). The PCR was carried out using SYBR™ Green master mix (Thermo Scientific, Finland) in a CFX384 Touch™ system (Bio-Rad, Finland). The primers used were designed in the NCBI database. The $2^{-\Delta\Delta Ct}$ method was used to calculate mRNA expression the relative to the housekeeping gene. The primer sequences are mentioned in **Supplementary Table 1**.

Western blotting

Cells were seeded on a 6-well plate at a density of 5.0×10^5 cells/well. In the case of 5-FU treatment, the following day after seeding, the culture medium was replaced with the medium containing 5-FU (IC_{50} as mentioned in Sect. 5.3.1). After 48 h, the cells were harvested in RIPA Buffer (Merck, Germany) with protease (ThermoFisher Scientific, USA) and phosphatase (ThermoFisher Scientific, USA) inhibitors. The protein concentration was measured using a bicinchoninic acid (BCA) protein assay (ThermoFisher Scientific, USA). The protein lysates were loaded at equal concentrations into each well, along with protein ladder (Biorad, Cat. 1610374 or Nippon Genetics, Cat. MWPO4). The samples were separated on 4–12% Mini-PROTEAN® TGX™ Precast Gels (Bio-Rad, Finland) and transferred onto the nitrocellulose membrane at 4 °C for 1.5 h at 100 V in Towbin transfer buffer. The membrane was blocked with blocking buffer [5% bovine serum albumin (BSA); Sigma-Aldrich, Finland] in Tris-buffered saline with 0.1% Tween-20 (TBST) for 1 h at room temperature (RT). The blocked membrane was incubated overnight at 4 °C with primary antibodies **(Supplementary Table 2)**. The membrane was washed in TBST (5min x 3) and incubated with anti-rabbit 800CW or anti-mouse 680CW secondary antibodies (IRDye® LI-COR Biosciences, US) for 1 h at room temperature. The signals from target proteins were visualized and quantitated using the Odyssey® CLx imaging system and software (LI-COR, USA). The original, uncropped images of the membranes are shown in **Supplementary Fig. 5**.

Cell cycle analysis

Cells were seeded on a 6-well plate at a density of 5.0×10^5 cells/well. The growth medium was replaced with the medium containing 5-FU (IC_{50} as mentioned in Sect. 5.3.1) after the cells were adhered. After 48 h of treatment, the cells were pelleted and washed with cold PBS. Further cell processing was performed using a Cell Cycle Analysis Kit (Abcam, ab287852) according to the manufacturer's protocol. The stained cells were analyzed with Cytoflex (Beckman Coulter) flow cytometer using CytExpert software (2.3.0.84). The acquisition rate was 200 events per second in medium acquisition mode, and at least 10,000 events were measured. The raw numerical data were processed using CytExpert software (2.3.0.84).

Organotypic 3D cultures

The organotypic 3D cultures were generated as described previously[17]. Briefly, the growth matrix was prepared using BD Matrigel™ (#356231 Corning, USA). 1000 cells/well were seeded in a 2:1 ratio of Matrigel (4 mg/ml) in the bottom and the upper layer (2 mg/ml) of the sandwich model in 96-well angiogenesis µ-plates (#89646, Ibidi, Germany). After 4 h of polymerization at 37 °C, each well was topped with growth media and monitored continuously for 10 days using IncuCyte S3 live-cell imaging. The organoids were maintained by the addition of fresh growth media every 2–3 days.

Drug treatment in 3D model

After 4 days of culturing and organoid formation, they were treated with 5-FU (IC_{50} as mentioned in Sect. 5.3.1). The growth medium supplemented with 5-FU or solvent DMSO (control) was renewed every 2–3 days up to day 10 of organoid growth.

3D organoid staining and confocal image acquisition

After 10 days of culturing, the organoids were stained with 1 µg/ml of Calcein AM (#C3099, ThermoFisher, Finland) to visualize the live cells (green fluorescence) and 1 µg/ml of Ethidium Homodimer-2 (red fluorescence; #E3599, ThermoFisher, Finland) to visualize the dead cells. The plate with stained organoids was incubated at 37 °C for 30 min and imaged using a spinning disk confocal microscope (3i CSU-W1, Zeiss 5x objective, Germany). Confocal stacks were acquired with the use of the Plan-Neofluar 5× objective. The images were processed using the SlideBook6 software (Intelligent Imaging Innovations Inc., USA).

Morphometric quantification of 3D organotypic culture

The images of the organoids obtained were segmented using the AMIDA software[57]. The raw numerical data providing morphometric measures including size or area (in pixels), shape or roundness (in percentage), and protrusions typical of invasion, such as appendages (in pixels), were statistically processed and visualized as graphs with R (version 3.6.2) within the Rstudio interface (http://www.r-project.org).

Cell viability assay in 3D model

The cells were seeded on the 96-well Ibidi plate and cultured as described in point 2.3. After the 5-FU treatment (IC_{50} as mentioned in Sect. 5.3.1), the viability was acquired using CellTiter-Glo® Luminescent Cell Viability Assay (Promega, USA) as per the manufacturer's protocol. The luminescence reading was measured using the VICTORX Light Luminescence Microplate Reader (Perkin Elmer, USA).

Immunofluorescence staining and quantification

The organoids were fixed with 4% paraformaldehyde, permeabilized with 0.5% Triton X-100, and blocked with 3% BSA. These organoids were washed with PBS and incubated with primary antibodies overnight. The dilutions of the antibodies are mentioned in **Supplementary Table 2.** Excess antibody was washed off with PBS and incubated with nuclear stain DAPI (450 nm, 1:1000; Thermo Fischer, Finland) along with a secondary antibody (goat anti-rabbit IgG-Alexa Flour Plus 488, Thermo Fischer Scientific, USA). The images were recorded with the 3i CSU-W1 spinning disk confocal microscope using Zeiss 40x/0.6 LD Plan-Neofluar objectives (3I GmbH, Germany). The organoids in the images were then segmented as objects using AMIDA. Their fluorescence was quantified by creating masks for each wavelength, obtaining the average voxel value in the object and the mask statistics in the SlideBook6 software (Intelligent Imaging Innovations Inc., USA).

Bioinformatics and statistical analysis

Gene expression profiling interactive analysis (GEPIA, http://gepia.cancer-pku.cn/help.html) was applied to analyze *SIRT7* expression in patient samples[58]. The correlation of *SIRT7* mRNA expression and SIRT7 protein expression in HNSCC was assessed using cBioPortal[59]. The data in all the experiments in this study are shown as the average of three biological replicates with ± standard deviation (SD). Statistical analyses were conducted in GraphPad Prism v. 9.0.0. (GraphPad Software Inc., USA). The statistical tests used are mentioned in the captions under each figure. Statistical differences were considered relevant at $p < 0.05$ (* $p < 0.05$, ** $p < 0.01$, *** $p < 0.001$, **** $p < 0.00001$ versus the control). Data on the graphs are expressed as mean ± standard deviation of the mean (± SD). When the ANOVA test was used, since we focused on the significance between controls and SIRT7-KO clones, we did not show statistical significance between clones.

Data availability

Data is provided within the manuscript or supplementary information files.

Received: 11 July 2024; Accepted: 13 December 2024
Published online: 16 January 2025

References

1. Siegel, R. L. et al. Cancer Statistics, 2023. *CA Cancer J. Clin.* **73**, 1, 17–48, doi: https://doi.org/10.3322/CAAC.21763. (2023).
2. Johnson, D. E. et al. Head and neck squamous cell carcinoma. *Nat. Rev. Dis. Primers*. **6**(1). https://doi.org/10.1038/S41572-020-00224-3 (2020).
3. Economopoulou, P., de Bree, R., Kotsantis, I. & Psyrri, A. Diagnostic Tumor Markers in Head and Neck Squamous Cell Carcinoma (HNSCC) in the Clinical Setting, *Front Oncol.* vol. 9, no. AUG, p. 827, doi: https://doi.org/10.3389/FONC.2019.00827 (2019).
4. Johnson, D. E. et al. Head and neck squamous cell carcinoma. *Nat. Rev. Dis. Primers* **6**(1), 92. https://doi.org/10.1038/S41572-020-00224-3 (2020).
5. Guigay, J. et al. Cetuximab, docetaxel, and cisplatin versus platinum, fluorouracil, and cetuximab as first-line treatment in patients with recurrent or metastatic head and neck squamous-cell carcinoma (GORTEC 2014-01 TPExtreme): a multicentre, open-label, randomised, phase 2 trial. *Lancet Oncol.* **22**(4), 463–475. https://doi.org/10.1016/S1470-2045(20)30755-5 (2021).
6. Lacas, B. et al. Meta-analysis of chemotherapy in head and neck cancer (MACH-NC): An update on 107 randomized trials and 19,805 patients, on behalf of MACH-NC Group. *Radiother Oncol.* **156**, 281. https://doi.org/10.1016/J.RADONC.2021.01.013 (2021).
7. Kakurina, G. V. et al. Expression of Genes Encoding Cell Motility Proteins during Progression of Head and Neck Squamous Cell Carcinoma. *Bull. Exp. Biol. Med.* **166**(2), 250–252. https://doi.org/10.1007/S10517-018-4325-1/METRICS (2018).
8. De Almeida, M. R., Pérez-Sayáns, M., Suárez-Peñaranda, J. M., Somoza-Martín, J. M. & García-García, A. p27Kip1 expression as a prognostic marker for squamous cell carcinoma of the head and neck. *Oncol. Lett.* **10**(5), 2675. https://doi.org/10.3892/OL.2015.3726 (2015).
9. Fayette, J. et al. Abemaciclib in recurrent/metastatic head and neck squamous cell carcinoma (RM-HNSCC) harboring CDKN2A loss, and/or CCND1 and/or CDK6 amplification: A phase II multicenter trial., https://doi.org/10.1200/JCO.2023.41.*16_suppl.6044*. vol. 41, no. 16_suppl, pp. 6044–6044. doi: https://doi.org/10.1200/JCO.2023.41.16_SUPPL.6044 (2023).
10. Pickering, C. R. et al. Mutational landscape of aggressive cutaneous squamous cell carcinoma. *Clin. Cancer Res.* **20**(24), 6582–6592. https://doi.org/10.1158/1078-0432.CCR-14-1768/270296/AM/MUTATIONAL-LANDSCAPE-OF-AGGRESSIVE-CUTANEOUS (2014).
11. Romanowska, K., Sobecka, A., Rawłuszko-Wieczorek, A. A., Suchorska, W. M. & Golusiński, W. Head and Neck Squamous Cell Carcinoma: Epigenetic Landscape. *Diagnostics* **11**(1), 34. https://doi.org/10.3390/DIAGNOSTICS11010034 (2021).
12. Castilho, R. M., Squarize, C. H. & Almeida, L. O. Epigenetic Modifications and Head and Neck Cancer: Implications for Tumor Progression and Resistance to Therapy. *Int. J. Mol. Sci.* **18**(7). https://doi.org/10.3390/IJMS18071506 (2017).
13. Hałasa, M. et al. H3K18Ac as a Marker of Cancer Progression and Potential Target of Anti-Cancer Therapy. *Cells* **8**(5). https://doi.org/10.3390/CELLS8050485 (2019).
14. Halasa, M. et al. Deacetylation of Transcription Factors in Carcinogenesis. *Int. J. Mol. Sci.* **22**, 11810. https://doi.org/10.3390/IJMS222111810 (2021).
15. Jin, Q. et al. Sirtuins in kidney diseases: potential mechanism and therapeutic targets. *Cell. Commun. Signal.* **22**(1). https://doi.org/10.1186/S12964-023-01442-4 (Dec. 2024).
16. Malik, S. et al. SIRT7 inactivation reverses metastatic phenotypes in epithelial and mesenchymal tumors. *Sci. Rep.* **5**(1), 9841. https://doi.org/10.1038/srep09841 (2015).
17. Zhang, S. et al. Sirt7 promotes gastric cancer growth and inhibits apoptosis by epigenetically inhibiting miR-34a. *Sci. Rep.* **5**(1), 9787. https://doi.org/10.1038/srep09787 (2015).
18. Barber, M. F. et al. SIRT7 links H3K18 deacetylation to maintenance of oncogenic transformation. *Nature* **487**, 114–118. https://doi.org/10.1038/nature11043 (2012).
19. Kaiser, A. et al. SIRT7: an influence factor in healthy aging and the development of age-dependent myeloid stem-cell disorders, *Leukemia*, vol. 34, no. 8, pp. 2206–2216. doi: https://doi.org/10.1038/s41375-020-0803-3 (2020).
20. Tang, X. et al. SIRT7 antagonizes TGF-β signaling and inhibits breast cancer metastasis. *Nat. Commun.* **8**(1). https://doi.org/10.1038/s41467-017-00396-9 (2017).
21. The potential of SIRT6 and SIRT7 as circulating markers for head and neck squamous cell carcinoma - PubMed. Accessed: Apr. 28. https://pubmed.ncbi.nlm.nih.gov/25503141/ (2024).
22. Lai, C. C. et al. Altered expression of SIRT gene family in head and neck squamous cell carcinoma. *Tumor Biol.* **34**(3), 1847–1854. https://doi.org/10.1007/S13277-013-0726-Y/METRICS (2013).
23. Zhou, W. H. et al. The Overexpression of Fibronectin 1 Promotes Cancer Progression and Associated with M2 Macrophages Polarization in Head and Neck Squamous Cell Carcinoma Patients. *Int. J. Gen. Med.* **15**, 5027. https://doi.org/10.2147/IJGM.S364708 (2022).
24. Choi, J. H. et al. Single-cell transcriptome profiling of the stepwise progression of head and neck cancer. *Nat. Commun.* **14**(1). https://doi.org/10.1038/S41467-023-36691-X (2023).
25. Fan, Z. et al. Targeting methyltransferase PRMT5 retards the carcinogenesis and metastasis of HNSCC via epigenetically inhibiting Twist1 transcription, *Neoplasia* vol. 22, no. 11, pp. 617–629. doi: https://doi.org/10.1016/J.NEO.2020.09.004 (2020).
26. Åkerfelt, M., Toriseva, M. & Nees, M. Quantitative Phenotypic Image Analysis of Three-Dimensional Organotypic Cultures. *Methods Mol. Biol.* **1612**, 433–445. https://doi.org/10.1007/978-1-4939-7021-6_31 (2017).
27. Dmello, C. et al. Vimentin-mediated regulation of cell motility through modulation of beta4 integrin protein levels in oral tumor derived cells. *Int. J. Biochem. Cell. Biol.* **70**, 161–172. https://doi.org/10.1016/J.BIOCEL.2015.11.015 (2016).

28. Baker, S. J., Poulikakos, P. I., Irie, H. Y., Parekh, S. & Reddy, E. P. CDK4: a master regulator of the cell cycle and its role in cancer. *Genes Cancer* **13**, 21. https://doi.org/10.18632/GENESANDCANCER.221 (2022).
29. Massacci, G., Perfetto, L. & Sacco, F. The Cyclin-dependent kinase 1: more than a cell cycle regulator, *British Journal of Cancer*. vol. 129, no. 11, pp. 1707–1716. doi: https://doi.org/10.1038/s41416-023-02468-8 (2023).
30. Huo, Q., Li, Z., Cheng, L., Yang, F. & Xie, N. SIRT7 Is a Prognostic Biomarker Associated With Immune Infiltration in Luminal Breast Cancer. *Front. Oncol.* **10**, 621. https://doi.org/10.3389/FONC.2020.00621 (2020).
31. Zhao, J. et al. SIRT7 regulates hepatocellular carcinoma response to therapy by altering the p53-dependent cell death pathway. *J. Exp. Clin. Cancer Res.* **38**(1). https://doi.org/10.1186/S13046-019-1246-4 (2019).
32. Yu, H. et al. Overexpression of Sirt7 exhibits oncogenic property and serves as a prognostic factor in colorectal cancer. *Clin. Cancer Res.* **20**(13), 3434–3445. https://doi.org/10.1158/1078-0432.CCR-13-2952/86289/AM/OVEREXPRESSION-OF-SIRT7-EXHIBITS-ONCOGENIC (2014).
33. Kim, J. K. et al. Sirtuin7 oncogenic potential in human hepatocellular carcinoma and its regulation by the tumor suppressors MiR-125a-5p and MiR-125b. *Hepatology* **57**(3), 1055–1067. https://doi.org/10.1002/HEP.26101 (2013).
34. Disruption of SIRT7 Increases the Efficacy of Checkpoint Inhibitor via MEF2D Regulation of Programmed Cell Death 1 Ligand 1 in Hepatocellular Carcinoma Cells - Gastroenterology. Accessed: Apr. 28. https://www.gastrojournal.org/article/S0016-5085(19)41477-7/fulltext?referrer=https%3A%2F%2Fwww.nature.com%2F (2024).
35. Tang, X. et al. SIRT7 antagonizes TGF-β signaling and inhibits breast cancer metastasis, *Nat. Commun.*, vol. 8, no. 1, pp. 1–14. doi: https://doi.org/10.1038/s41467-017-00396-9 (2017).
36. Han, Y. et al. Hsa-miR-125b suppresses bladder cancer development by down-regulating oncogene SIRT7 and oncogenic long non-coding RNA MALAT1. *FEBS Lett.* **587**, 3875–3882. https://doi.org/10.1016/J.FEBSLET.2013.10.023 (2013).
37. Ding, M. et al. SIRT7 depletion inhibits cell proliferation and androgen-induced autophagy by suppressing the AR signaling in prostate cancer. *J. Exp. Clin. Cancer Res.* **39**(1). https://doi.org/10.1186/S13046-019-1516-1 (2020).
38. Gu, Y. et al. SIRT7 promotes Hippo/YAP activation and cancer cell proliferation in hepatocellular carcinoma via suppressing MST1. *Cancer Sci.* **115**(4). https://doi.org/10.1111/CAS.16091 (2024).
39. Kavitha, L. et al. Expression of CD44 in Head and Neck Squamous Cell Carcinoma—An In-Silico Study. *Glob Med. Genet.* **10**(3), 221. https://doi.org/10.1055/S-0043-1772459 (2023).
40. Zhou, W. H. et al. The Overexpression of Fibronectin 1 Promotes Cancer Progression and Associated with M2 Macrophages Polarization in Head and Neck Squamous Cell Carcinoma Patients. *Int. J. Gen. Med.* **15**, 5027–5042. https://doi.org/10.2147/IJGM.S364708 (2022).
41. Khales, S. A., Mozaffari-Jovin, S., Geerts, D. & Abbaszadegan, M. R. TWIST1 activates cancer stem cell marker genes to promote epithelial-mesenchymal transition and tumorigenesis in esophageal squamous cell carcinoma. *BMC Cancer* **22**(1), 1–14. https://doi.org/10.1186/S12885-022-10252-9/FIGURES/7 (2022).
42. Nguyen, P. T. et al. N-cadherin expression is involved in malignant behavior of head and neck cancer in relation to epithelial-mesenchymal transition. *Histol. Histopathol.* **26**(2), 147–156. https://doi.org/10.14670/HH-26.147 (2011).
43. Li, W., Zhu, D. & Qin, S. SIRT7 suppresses the epithelial-to-mesenchymal transition in oral squamous cell carcinoma metastasis by promoting SMAD4 deacetylation. *J. Experimental Clin. Cancer Res.* **37**(1), 1–11. https://doi.org/10.1186/S13046-018-0819-Y/TABLES/1 (2018).
44. Battaglia, R. A., Delic, S., Herrmann, H. & Snider, N. T. Vimentin on the move: new developments in cell migration, *F1000Res*, vol. 7. doi: https://doi.org/10.12688/F1000RESEARCH.15967.1 (2018).
45. Lu, Y. F. et al. SIRT7 activates p53 by enhancing PCAF-mediated MDM2 degradation to arrest the cell cycle. *Oncogene* **39**, 4650. https://doi.org/10.1038/S41388-020-1305-5 (2020).
46. de Bakker, T. et al. Restoring p53 Function in Head and Neck Squamous Cell Carcinoma to Improve Treatments. *Front. Oncol.* **11**. https://doi.org/10.3389/FONC.2021.799993 (2021).
47. Zhao, Y. et al. Sirtuin 7 promotes non-small cell lung cancer progression by facilitating G1/S phase and epithelial-mesenchymal transition and activating AKT and ERK1/2 signaling. *Oncol. Rep.* **44**(3), 959. https://doi.org/10.3892/OR.2020.7672 (2020).
48. Vazquez, B. N. et al. SIRT 7 promotes genome integrity and modulates non-homologous end joining DNA repair. *EMBO J.* **35**(14), 1488–1503. https://doi.org/10.15252/EMBJ.201593499/SUPPL_FILE/EMBJ201593499-SUP-0003-SDATAFIGEV.ZIP (2016).
49. Strzalka, P. et al. Assessment of SIRT1-SIRT7 and TP53 Genes Expression in Patients with Acute Myeloid Leukemia, *Blood* vol. 142, no. Supplement 1, pp. 6048–6048. doi: https://doi.org/10.1182/BLOOD-2023-187756 (2023).
50. Noguchi, A. et al. SIRT1 expression is associated with good prognosis for head and neck squamous cell carcinoma patients. *Oral Surg. Oral Med. Oral Pathol. Oral Radiol.* **115**(3), 385–392. https://doi.org/10.1016/J.OOOO.2012.12.013 (2013).
51. Ijichi, K. et al. Pretreatment with 5-FU enhances cisplatin cytotoxicity in head and neck squamous cell carcinoma cells. *Cancer Chemother. Pharmacol.* **62**(5), 745–752. https://doi.org/10.1007/s00280-007-0658-6 (2008).
52. Billard-Sandu, C. et al. CDK4/6 inhibitors in P16/HPV16-negative squamous cell carcinoma of the head and neck. *Eur. Arch. Otorhinolaryngol.* **277**(5), 1273–1280. https://doi.org/10.1007/S00405-020-05891-2 (2020).
53. Chen, M. et al. Research progress on Sirtuins (SIRTs) family modulators. *Biomed. Pharmacother* **174**. https://doi.org/10.1016/J.BIOPHA.2024.116481 (2024).
54. Bolding, J. E. et al. Substrates and Cyclic Peptide Inhibitors of the Oligonucleotide-Activated Sirtuin 7. *Angew Chem. Int. Ed. Engl.* **62**(49). https://doi.org/10.1002/ANIE.202314597 (2023).
55. Ran, F. A. et al. Genome engineering using the CRISPR-Cas9 system, *Nature Protocols 2013 8:11*, vol. 8, no. 11, pp. 2281–2308. doi: https://doi.org/10.1038/nprot.2013.143 (2013).
56. Engler, C., Gruetzner, R., Kandzia, R. & Marillonnet, S. Golden Gate Shuffling: A One-Pot DNA Shuffling Method Based on Type IIs Restriction Enzymes. *PLoS One* **4**(5), e5553. https://doi.org/10.1371/JOURNAL.PONE.0005553 (2009).
57. Härmä, V. et al. Quantification of Dynamic Morphological Drug Responses in 3D Organotypic Cell Cultures by Automated Image Analysis. *PLoS One* **9**(5), e96426. https://doi.org/10.1371/JOURNAL.PONE.0096426 (2014).
58. Tang, Z. et al. GEPIA: a web server for cancer and normal gene expression profiling and interactive analyses. *Nucleic Acids Res.* **45**, W98–W102. https://doi.org/10.1093/NAR/GKX247 (2017). no. W1.
59. Gao, J. et al. Integrative analysis of complex cancer genomics and clinical profiles using the cBioPortal. *Sci. Signal.* **6**(269). https://doi.org/10.1126/SCISIGNAL.2004088 (2013).

Acknowledgements

We would like to acknowledge Jesse Mattsson from the University of Turku for technical assistance with confocal microscopy.

Author contributions

M. H.: Conceptualization, Data curation, Formal analysis, Investigation, Methodology, Software, Writing original draft, Review & Editing. S.A.: Conceptualization, Data curation, Formal analysis, Investigation, Methodology, Software, Writing original draft, Review & Editing. A.W.: Data Curation, Investigation, Methodology, Review, Supervision. A.B.: Data Curation, Investigation, Methodology. K. B.: Data curation, Investigation, Meth-

odology. A.P-P: Investigation, Methodology. J. K.: Investigation, Methodology. M.B.: Investigation, Methodology. A.R-M: Review, Supervision, Financial support, A.S.: Review, Supervision, Financial support, M.N.: Review, Supervision, Financial support.

Funding
This research was funded by The Polish National Agency for Academic Exchange, Poland, grant number PPN/IWA/2019/1/00160 and PPI/APM/2019/1/00089/U/00001 (M.H, A.S, M.N); the Polish National Science Centre (NCN) grant DEC-2017/25/B/NZ4/02364 (ARM); Jane and Aatos Erkko foundation, grant number 2600514111 (S.A, M.N); Turku University Foundation/Turun Yliopistosäätiö (080956, S.A.); Drug Research Doctoral Program, University of Turku (S.A); the Finnish-Norwegian Medical Foundation/ Suomalais- Norjalainen Lääketieteen Säätiö (2024043, S.A.); Ida Montinin Säätiö, Finland (20240522,S.A).

Declarations

Competing interests
The authors declare no competing interests.

Additional information
Supplementary Information The online version contains supplementary material available at https://doi.org/10.1038/s41598-024-83349-9.

Correspondence and requests for materials should be addressed to M.H. or A.W.